Biol. Cybern. 84, 133–141 (2001)

Biological Cybernetics

Analysis of the reflexive feedback control loop during posture maintenance

Erwin de Vlugt, Frans C. T. van der Helm, Alfred C. Schouten, Guido G. Brouwn

Man-Machine Systems and Control, Department of Mechanical Engineering, Delft University of Technology, Mekelweg 2, 2628 CD Delft, The Netherlands

Received: 24 January 2000 / Accepted in revised form: 7 July 2000

Abstract. In previous work it has been shown in posture experiments of the human arm that reflexive dynamics were substantial for narrow-band stochastic force disturbances. The estimated reflex gains varied substantially with the frequency content of the disturbances. The present study analyses a simplified linear model of the reflexive feedback control loop, to provide an explanation for the observed behaviour. The model describes co-activation and reflexive feedback. The task instruction 'minimize the displacements' is represented mathematically by a cost function that is minimized by adjusting the parameters of the model. Small-amplitude displacements allow the system to be analysed with a quasi-linear approach. The optimization results clarify the limited effectiveness of reflexive feedback on the system's closed-loop behaviour, which emanates from the time delay present in the reflex loops. For low-frequency inputs less than 5 Hz, boundary-stable solutions with high reflex gains are predicted to be optimal. Input frequencies near the system's eigenfrequency (about 5 Hz), however, would be amplified and result in oscillatory behaviour. As long as the disturbance does not excite these frequencies, boundary stability will be optimal. The predicted reflex gains show a striking similarity with the estimated reflex gains from the experimental study. The present model analysis also provides a clear explanation for the negative reflex gains, estimated for near-sinusoidal inputs beyond 1.5 Hz.

1 Introduction

The aim of the present study was to explain the estimated reflex gains during human arm posture tasks (F.C.T. van der Helm, submitted, 2000), by using an optimal control approach to analyse the closed-loop behaviour of a simplified linear model of the neuro-musculo-skeletal (NMS) system. Optimal control is a common tool in system engineering practice to design a controller which optimizes the system's response.

The subjects in these experiments were asked to 'minimize displacements' while small-amplitude stochastic force perturbations were applied to the hand with the aid of a compliant, linear hydraulic manipulator. Hand displacements were allowed only in the sagittal plane in anterior-posterior directions. Under these constraints the largest movement occurred around the shoulder joint. Because most natural posture tasks require the maintenance of an equilibrium position, force disturbances were applied, leaving a position task that required active stabilization. It is believed that under such conditions, the stabilizing role of spinal reflexes is studied best (Wieneke 1972; Fitzpatrick et al. 1992). The equilibrium position and the actual hand position were presented on a display to give the subject a clear perception of the task and prevent the hand drifting from the equilibrium position. The visual feedback with its long time delay of approximately 0.2 s (McRuer and Jex 1967) is most likely not effective for force disturbances above 1 Hz and therefore does not contribute to the performance of the task for these frequencies.

Since a NMS system is highly non-linear (Agarwal and Gottlieb 1977a,b, 1985; Kirsch et al. 1994), the features of the disturbance signal will have a large impact on the behaviour identified. In the experiments the stochastic perturbations excluded voluntary responses and were small enough to enable a quasi-linear approach in order to facilitate system identification (Kearney and Hunter 1990). From the experimental data, a linear describing function of the human arm dynamics was estimated by means of a closed-loop identification method. This function describes the dynamic relation between the hand position and the applied force disturbance in the frequency domain. A method was developed to identify intrinsic and reflexive components from the estimated describing function. This method shows that it is very plausible to assume invariant intrinsic behaviour with

Correspondence to: E. de Vlugt
(Tel.: +31-15-2785247, Fax: +31-15-2784717
e-mail: e.devlugt@wbmt.tudelft.nl)

varying frequency content of the applied force perturbations. Any difference in response, as obtained from the estimated describing function, is then accounted for by reflexive feedback. The estimated reflex gains varied strongly with the input spectral bandwidth. For input spectra containing only low frequencies, significant reflex gains were estimated. This seems plausible considering the time delays present in the reflex loops. High reflex gains were only effective for low-frequency inputs that did not excite the closed-loop system's eigenfrequency. High-frequency inputs close to the eigenfrequency would be amplified when the reflex gains were high. The gains decreased gradually, and reached zero around 3 Hz as the input bandwidth increased. For near-sinusoidal inputs, significant negative reflex gains were estimated for input frequencies beyond 1.5 Hz. Clearly, a system dynamics approach is indispensable when studying the stability issues underlying the observed behaviour.

Several theoretical studies of the postural control loop consider a system dynamics approach. Hogan (1984) predicts the optimal parameters of a simplified antagonistic muscle model, by minimizing a criterion function that weights performance and metabolic energy consumption. However, this model does not describe reflexive feedback and represents only co-activation of the muscles. Stein and Oğuztöreli (1984) simulate the impulse response of an antagonistic muscle model, including reflexive pathways between motor neurons and several inter neurons, by stimulating these neurons. Unfortunately, it is difficult to validate these results by means of similar experiments in intact systems during natural behaviour. Therefore, it is desirable to consider models with more simplified descriptions of reflexive feedback which can be validated by means of disturbance experiments with intact systems. Yurkovich et al. (1987) analyze the frequency response of a model describing a single stretch reflex loop. However, no explanation is provided for the relation between behaviour and goal of the system. Rozendaal (1997) optimizes the parameters of a model describing three reflex loops with position, velocity and force feedback. The goal of the system is assumed to be the realization of a pre-specified dynamic behaviour, which is represented in a criterion function. This is an alternative optimal control hypothesis of the adaptive behaviour of the central nervous system (CNS).

Optimal control theory predicts a relation between the experimental variables and the reflexive feedback gains. It assumes that the goal of the CNS is to minimize a criterion function. Evidence for this hypothesis is obtained by comparing predicted and estimated reflexive responses. Agreement between predicted and estimated behaviour is associated with the following conditions: (1) the criterion function is a valid representation of the task instruction, (2) the model is a valid representation of the real system, constraints and experimental conditions, and (3) the separation method estimates valid intrinsic and reflexive components.

The postural control loop is dominated by the (inter)action of mechanical muscle and joint properties, and spinal (stretch) reflexes. Mechanical stiffness and damping of joints increase simultaneously with the level of co-activation of opposing muscles. The gains of reflexive length and velocity feedback can be adjusted independently to optimize the response of the controlled system. The present study considers co-activation and reflex gains to be the primary parameters for postural control. Since co-activation influences the visco-elastic properties, high co-activation levels will effectively reduce the effects of external disturbances. The reflex gains, however, are not purely mechanical. Due to the time delays and the muscle activation phase lags in the reflex loops, high reflex gains will tend to destabilize the system by introducing oscillatory behaviour.

2 Model development

The dynamics of the postural control loop are linearized, describing the basic intrinsic and reflexive postural control mechanisms of the CNS for small variations of the variables around an equilibrium position x_d and a static muscle activation level u_0. The frequency-domain representation of the linear model is shown in Fig. 1, with $s = \lambda + j2\pi f$ where f is the frequency in Hz. It is assumed that $\lambda = 0$, because the initial transient response is not important.

The model parameters used are chosen to reasonably match the experimental results (Table 1). The linkage system is described by a second-order system $H_l(s)$, representing the inertia m_a and passive visco-elastic properties b_q and k_q:

$$H_l(s) = \frac{1}{m_a s^2 + b_q s + k_q} \tag{1}$$

The intrinsic feedback control loop $H_i(s)$ represents the simultaneous increase in mechanical muscle stiffness and damping by co-activation, around a certain muscle length and around zero muscle velocity. This is described by co-activation gain u_0:

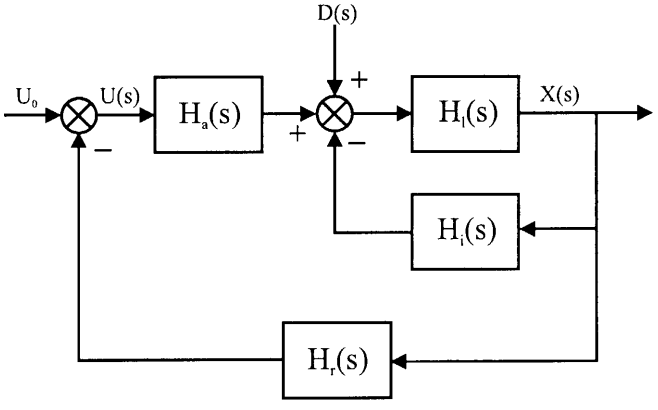

Fig. 1. Linear model of the postural control loop, consisting of an intrinsic feedback loop $H_l(s)$ and $H_i(s)$, and a reflexive feedback control loop $H_r(s)$ and $H_a(s)$. U_0 is the static muscle activation level, $U(s)$ is the result of U_0 and reflexive feedback, $D(s)$ is the external force disturbance and $X(s)$ is the hand position

Table 1. Parameters of the postural control loop model (F.C.T. van der Helm, submitted, 2000)

	Value	Unit	Description
m_a	2	kg	Arm mass
b_q	15	Ns/m	Passive damping
k_q	180	N/m	Passive stiffness
b_m	30	Ns/m	Intrinsic damping coefficient
k_m	650	N/m	Intrinsic stiffness coefficient
τ_a	55	ms	Activation time constant
T_d	40	ms	Neural time delay
u_0	–	–	Co-activation level
k_p	–	N/m	Reflexive position feedback gain
k_v	–	Ns/m	Reflexive velocity feedback gain
δ	0.05	–	Smallest stability margin

$$H_i(s) = (b_m s + k_m)u_0 \tag{2}$$

with $0 \le u_0 \le 1$. The reflexive feedback control loop is described by receptor dynamics $H_r(s)$ and by muscle activation dynamics $H_a(s)$. $H_r(s)$ represents the position sensitivity k_p, the velocity sensitivity k_v of muscle spindles, and the conduction time delays T_d:

$$H_r(s) = (k_v s + k_p)e^{-sT_d} \tag{3}$$

Reflexive force feedback is also incorporated in the model. However, force feedback appears not to be relevant to the present analysis (see Sect. 4). Consequently, the description of force feedback is omitted here for clarity. Muscle activation to force build-up is represented by a first-order process with activation time constant $\tau_a = 55$ ms. This is a reasonable approximation of two linear first-order processes in series, representing the excitation and activation dynamics with time constants of 40 ms and 30 ms (e.g. Winters and Stark 1985; Winters et al. 1988), respectively:

$$H_a(s) = \frac{1}{\tau_a s + 1} \tag{4}$$

The intrinsic dynamics, (1) and (2), represent the musculo-skeletal system, and can be considered to be controlled by reflexive feedback. Therefore, in order to analyze the reflexive feedback loop, the intrinsic dynamics are lumped into the 'plant' dynamics $H_p(s)$:

$$H_p(s) = \frac{H_l(s)}{1 + H_l(s)H_i(s)} \tag{5}$$

whereas the reflexive dynamics are lumped into the 'controller' dynamics $H_c(s)$:

$$H_c(s) = H_a(s)H_r(s) \tag{6}$$

The overall behaviour is described by the closed-loop transfer function $H_{CL}(s)$:

$$H_{CL}(s) = \frac{X(s)}{D(s)} \tag{7}$$

$$= \frac{H_p(s)}{1 + H_p(s)H_c(s)} \tag{8}$$

and including (1–6) gives:

$$H_{CL}(s) = \frac{\tau_a s + 1}{(\tau_a s + 1)(m_a s^2 + b_q s + k_q + (b_m s + k_m)u_0) + (k_v s + k_p)e^{-sT_d}} \tag{9}$$

The stability properties are described by the open-loop transfer function $H_{OL}(s)$:

$$H_{OL}(s) = H_p(s)H_c(s) \tag{10}$$

Again, including (1–6) gives:

$$H_{OL}(s) = \frac{(k_v s + k_p)e^{-sT_d}}{(\tau_a s + 1)(m_a s^2 + b_q s + k_q + (b_m s + k_m)u_0)} \tag{11}$$

3 Methods

3.1 Cost function

The task instruction 'minimize the displacements' is represented mathematically in the form of a cost function to be minimized. Having a linear, noise-free system with stationary stochastic inputs, the cost function J of the displacement $x(t)$ is:

$$J = E\{x^2(t)\} \tag{12}$$

where $E\{\cdot\}$ is the expectation operator. When $E\{x(t)\} = 0$, J is the variance σ_x^2 of $x(t)$. By using the following relations:

$$J = \sigma_x^2 = \int_{-\infty}^{\infty} S_{xx}(f)\mathrm{d}f = 2 \cdot \int_{0^+}^{\infty} S_{xx}(f)\mathrm{d}f$$

and

$$S_{xx}(f) = E\{X(f) \cdot X(-f)\}$$
$$X(f) = H_{CL}(f) \cdot D(f)$$

J can be rewritten in the frequency domain:

$$J = 2 \cdot \int_{0^+}^{\infty} |H_{CL}(f)|^2 S_{dd}(f)\mathrm{d}f \tag{13}$$

$S_{dd}(f)$ is the power spectrum of the input signal. The system inputs have rectangular power spectra:

$$S_{dd}(f) = c \quad \forall\, f_l \le f \le f_h \ , \tag{14}$$

and zero elsewhere, so that J can be written as:

$$J = 2c \cdot \int_{f_l}^{f_h} |H_{CL}(f)|^2 \,\mathrm{d}f \tag{15}$$

Now J depends only on the gain of the closed-loop dynamics inside the input frequency range. Equation (15) indicates that, in order to minimize J, the closed-loop gain (squared) must be minimized but only for $f_l \leq f \leq f_h$. Consequently, the closed-loop behaviour outside the input frequency range is not relevant except for the closed-loop stability constraint (see Sect. 2) which is determined by the amplitude and phase margins of $H_{OL}(f)$. The interesting question is now: what values of the co-activation gain and reflex gains minimize J for a given input spectrum $\{f_l, f_h\}$? Minimizing the gain of $H_{CL}(s)$ requires maximization of u_0, k_p and k_v, as can be seen from (9).

The stability properties can be obtained from $H_{OL}(s)$. The system is stable if the Nyquist plot of $H_{OL}(s)$ does not encircle the point $(-1, 0)$. Equation (11) indicates that u_0 increases the gain margin, i.e. it stabilizes the system. Therefore, $u_0 = 1$ will be the optimal solution. However, the reflex gains decrease the gain margin, and must be limited to maintain stability since the presence of the time delay and the activation dynamics cause the phase of $H_{OL}(s)$ to shift beyond -180 degrees.

3.2 Parameter optimization

The parameters of the postural control model will be optimized by minimizing the cost function in (15). For the incorporation of the stability constraint, it is convenient to consider a state-space representation of the closed-loop transfer function in (8):

$$\begin{aligned} \dot{\mathbf{x}}_{nms}(t) &= A_{nms}\mathbf{x}_{nms}(t) + B_{nms}d(t) \\ x(t) &= C_{nms}\mathbf{x}_{nms}(t) \end{aligned} \tag{16}$$

where $\mathbf{x}_{nms}(t)$ is the state vector. The state matrices A_{nms}, B_{nms} and C_{nms} specify the relation between the system input $d(t)$ and the model output $x(t)$. The time delay is in theory an infinite order system, and must therefore be approximated by a low-order filter in a finite-order state-space representation. In this study a third-order Padé filter (Marshall 1979) is used. Consequently, $\mathbf{x}_{nms}(t)$ is a 6×1 vector, composed of $x(t)$, $\dot{x}(t)$, the activation state and the three Padé filter states. Equation (15) is computed by integrating numerically over f. Hereby, $H_{CL}(f)$ is computed either from (9) or from the frequency-domain equivalent of (16), i.e.:

$$H_{CL}(s) = C_{nms}(sI - A_{nms})^{-1}B_{nms} \tag{17}$$

The size of the identity matrix I equals the size of A_{nms}. Stability of the system is incorporated by a constraint on the eigenvalues of A_{nms}. The system is stable if all eigenvalues have a negative real value:

$$\max(\text{real}(\text{eig}(A_{nms}))) \leq -\delta \tag{18}$$

When $\delta = 0$, one or more eigenvalues have only an imaginary part, which corresponds with a boundary-stable system. This will introduce numerical problems which can be prevented when δ has a small positive value (Table 1). Regarding the input signals, two different types of narrow-bandwidth (NB) noise are considered:

1. NB noise type 1: $f_l = 0.05$ Hz whereas f_h is variable
2. NB noise type 2: $f_l = f_c - 0.15$ Hz and $f_h = f_c + 0.15$ Hz whereas f_c is variable

4 Results

4.1 Optimized reflex gains

The optimized reflex gains are shown in Fig. 2A and 2B. The optimal value for the co-activation gain is $u_0 = 1$ for all inputs. Force feedback did not contribute to increase the performance for all disturbance conditions because either the estimated force reflex gains became very small or the convergence of the gains was poor. This suggests that the reflexive force feedback is ineffective for the current task.

For comparison the average reflex gains k_p and k_v, estimated from the experiments over five subjects, are also shown in Fig. 2C and 2D. For NB noise type 1, f_h is varied between 0.8 and 3.8 Hz whereas for NB noise type 2, f_c is varied between 0.5 and 7 Hz.

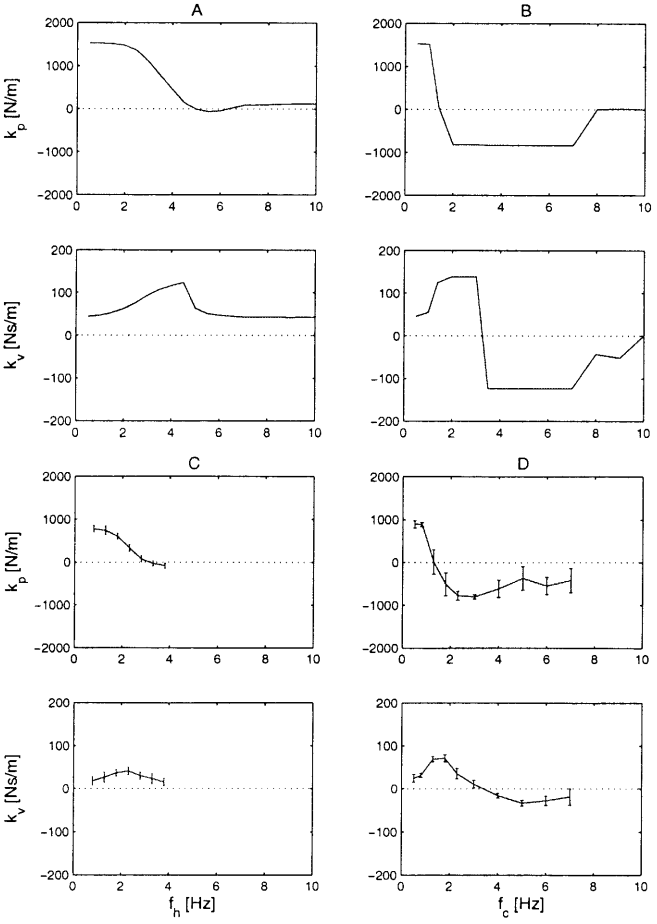

Fig. 2A,B. Optimized reflex gains: **A** narrow-bandwidth (NB) noise type 1; **B** NB noise type 2. **C, D**. Average reflex gains (*solid curves*), estimated from the experiments, plus and minus the SD over five subjects (*error bars*): **C** NB noise type 1; **D** NB noise type 2

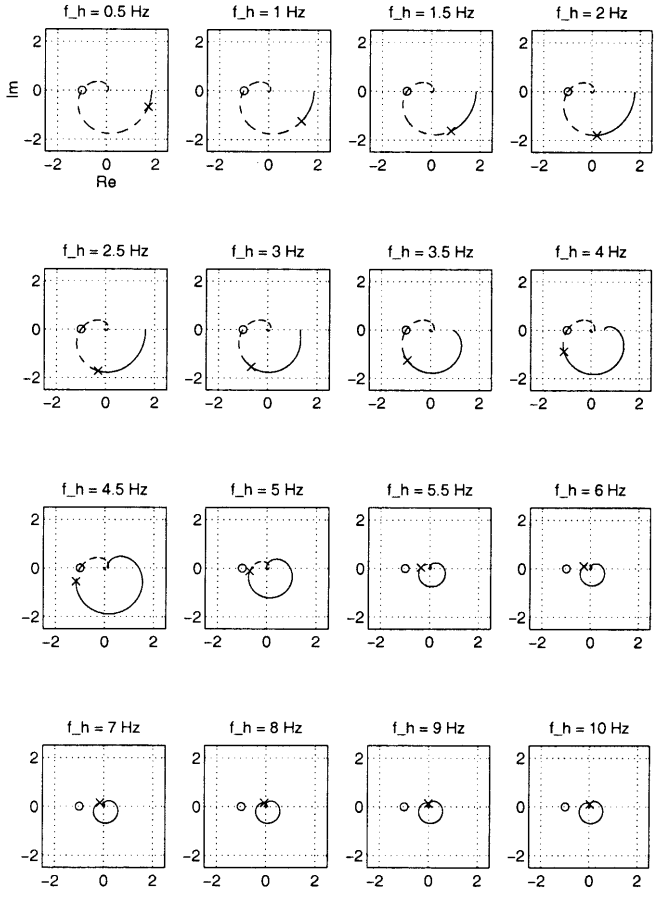

Fig. 3. Nyquist plots of $H_{OL}(f)$ for NB noise type 1 with different values of f_h. The *solid curves* denote the frequency range between f_l and f_h. The *crosses* denote f_h. The *circle* denotes the point $(-1, 0)$

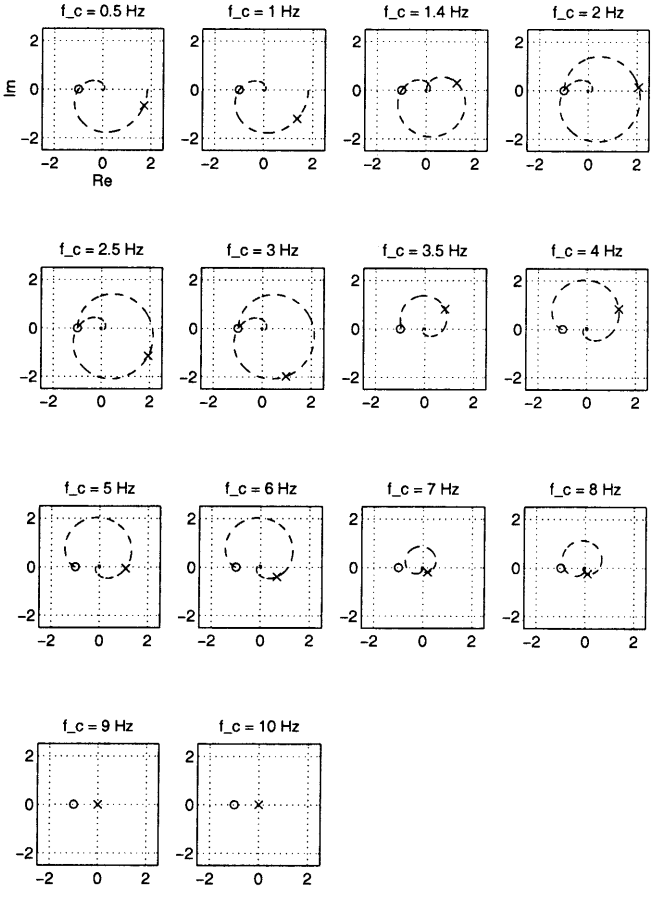

Fig. 4. Nyquist plots of $H_{OL}(f)$ for NB noise type 2 with different values of f_c, denoted by the *crosses*. The *circle* denotes the point $(-1, 0)$

4.2 Open-loop and closed-loop behaviour

In Figs. 3 and 4 the Nyquist plots of $H_{OL}(f)$ are shown, corresponding to the optimized model parameters. To guarantee stability, the Nyquist plot may not encircle the point $(-1, 0)$. It is indicated which part of the Nyquist plot corresponds with the input frequency range.

In Figs. 5 and 6 the magnitudes of $H_{CL}(f)$ are shown, corresponding to the optimized model parameters. As a reference, the gains of $H_{CL}(f)$ of the intrinsic model ($H_c(f) = 0$) are also plotted.

In Figs. 7 and 8 the magnitudes of the estimated transfer functions for both NB noise type 1 and type 2 are shown for one subject. As a reference the gains which correspond with wide-bandwidth (WB) noise ($f_l = 0.05$ Hz and $f_h = 20$ Hz) as input, are also plotted. For WB noise, only intrinsic dynamics were estimated. In these figures the corresponding input frequency ranges are also indicated.

5 Discussion

The optimized and estimated reflex gains in Fig. 2, and especially k_p, show a surprisingly comparable variation with the input spectral bandwidth, whereas their values have the same order of magnitude. The Nyquist plots of $H_{OL}(f)$ and the Bode plots of $|H_{CL}(f)|$ provide a visual interpretation of how the optimal reflex gains affect the stability of the system.

5.1 NB noise type 1, signals with increasing bandwidth

It is evident that the solutions for low-frequency inputs are boundary-stable, because $H_{OL}(f)$ touches the point $(-1, 0)$. The solutions are still optimal, since the frequencies around the point $(-1, 0)$ are not excited by the input signal. On the one hand, input frequencies close to the point $(-1, 0)$ are highly amplified and will result in oscillatory behaviour. On the other hand, input frequencies far from the point $(-1, 0)$ will be suppressed (see also Eq. 8). Therefore it is beneficial to maximize the distance between $H_{OL}(f)$ and the point $(-1, 0)$ in the frequency region where the input signal excites the system (McRuer and Jex 1967). This is what happens in Fig. 3. For low-frequency inputs, k_p is maximized such that $H_{OL}(f)$ is located far from the point $(-1, 0)$, whereas the system is boundary stable. However, as the input bandwidth increases, at some point between $f_h = 4.5$ Hz and $f_h = 5$ Hz, $H_{OL}(f)$ approaches the point $(-1, 0)$. Beyond this point k_p is no longer effective

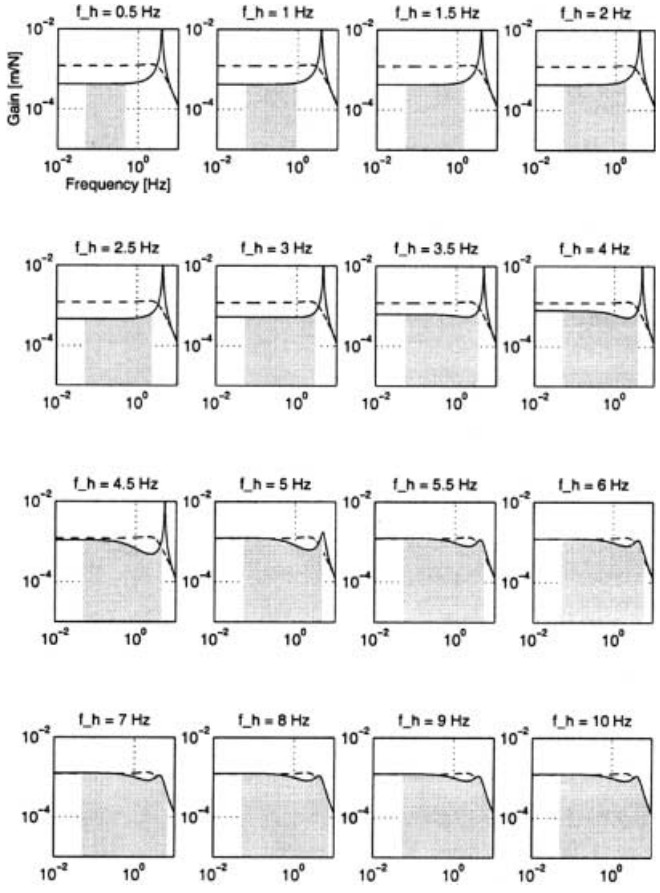

Fig. 5. Magnitudes of $H_{CL}(f)$ for NB noise type 1 with different values of f_h (*solid curves*), and for $H_c(f) = 0$, i.e. only intrinsic feedback (*dashed curves*). The *filled areas* denote the frequency range between f_l and f_h

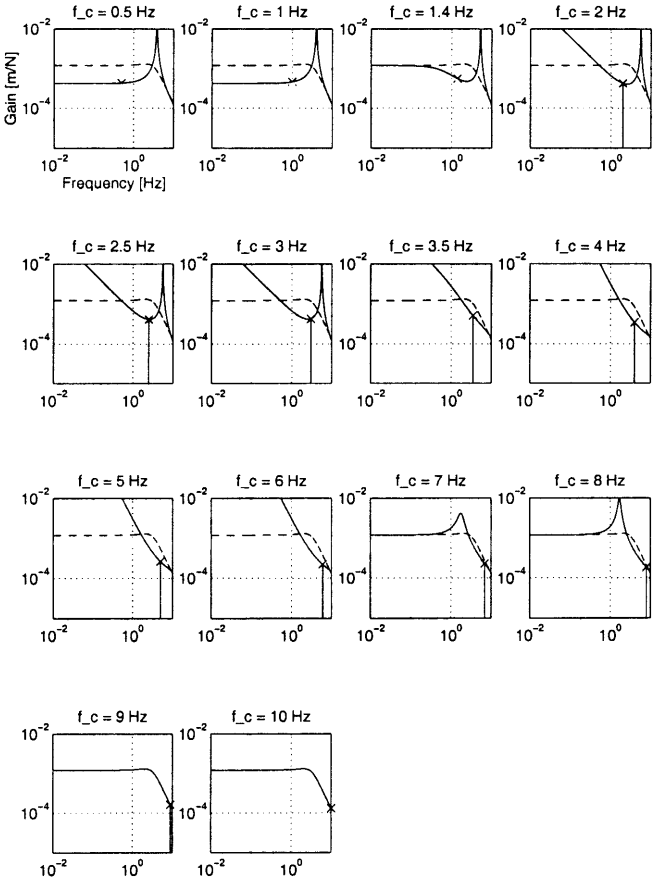

Fig. 6. Magnitudes of $H_{CL}(f)$ for NB noise type 2 with different values of f_c (*solid curves*), and for $H_c(f) = 0$, i.e. only intrinsic feedback (*dashed curves*). The *crosses* denote f_c

and decreases to zero. The role of k_v is to increase the phase margin of $H_{OL}(f)$, i.e. rotating the Nyquist plot counterclockwise. This will result in a phase lead, i.e. increasing the distance to the point $(-1, 0)$. As shown in Fig. 5 for the closed-loop system H_{CL}, the boundary-stable solutions between $f_h = 0.5$ Hz and $f_h = 4.5$ Hz clearly introduce the resonant peak between 4 Hz and 5 Hz, the so-called eigenfrequency. Beyond the eigenfrequency, high reflex gains would lead to an increase in the area under the closed-loop gain by the resonant peak. Low reflex gains eliminate this peak.

5.2 NB noise type 2, near-sinusoidal signals with increasing center frequency

Most solutions are boundary-stable. In this case, for optimal behaviour it is beneficial to maximize the distance between the cross and the circle in Fig. 4. Up to about 1 Hz, the situation is identical to the NB noise type 1 case. Between $f_c = 2$ Hz and $f_c = 3$ Hz, the phase shift in the low-frequency part of $H_{OL}(f)$ becomes positive. In this case k_p has a maximally negative value, introducing a phase shift of +180 degrees, and projects the Nyquist plot for $f = 0$ onto the point $(-1, 0)$ (this

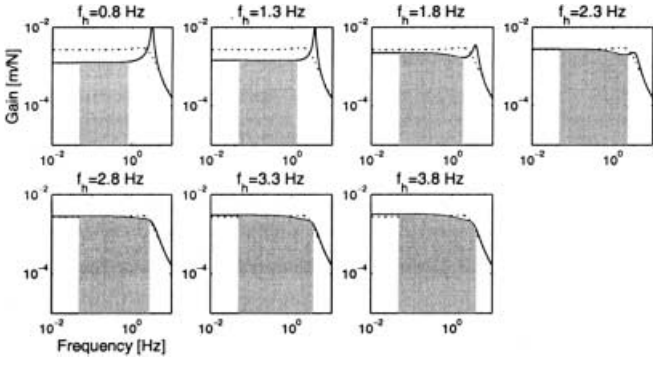

Fig. 7. Magnitudes of modelled closed-loop transfer function for subject NS: for NB noise type 1 with different values of f_h (*solid curves*), and for wide-bandwidth (WB) noise (*dashed curves*). The *filled areas* denote the frequency range between f_l and f_h

means that $k_p/(k_q + k_m) = -1$, i.e. $k_p = -830$ N/m). Notice that this solution is not effective for NB type 1 noise, because it would result in amplification of the low input frequencies! Between 3.5 Hz and 7 Hz, both k_p and k_v have a maximally negative value. This implies that the Nyquist plot with positive reflex gains is shifted by -180 degrees. This solution clearly keeps away the cross from the point $(-1, 0)$ as the center frequency

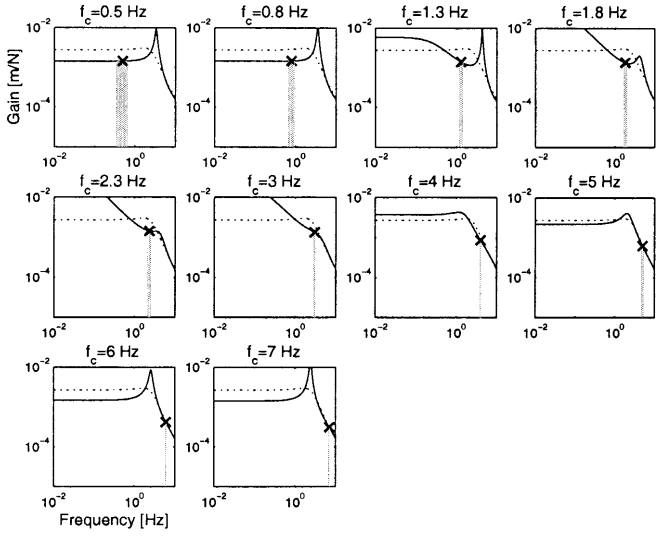

Fig. 8. Magnitudes of modelled closed-loop transfer function for subject NS: for NB noise type 2 with different values of f_c (*solid curves*), and for WB noise (*dashed curves*). The *crosses* denote f_c

increases, and is only effective for NB noise type 2. According to (15), the closed-loop gain must be minimal for $f \approx f_c$, which is illustrated in Fig. 6. In Fig. 4, the negative reflex gains between $f_c = 2$ Hz and $f_c = 6$ Hz locate the Nyquist plot for $f = 0$ near the point $(-1, 0)$. Consequently, the magnitude of $H_{CL}(f)$ is very large for low frequencies, whereas it is minimal near $f = f_c$.

5.3 Comparison with experimental results

The model optimization approach results in a maximal co-activation gain, independent of the input spectrum. This result is consistent with the assumption in the separation method to estimate intrinsic and reflexive dynamics, yielding that the intrinsic dynamics are constant and independent of the input spectrum. The experiments show essentially the same reflexive behaviour as predicted by the theoretical study. The predicted k_p and k_v show striking similarities with the estimated reflex gains (Fig. 2). For NB noise type 1, k_p decreases gradually to zero as f_h increases. For NB noise type 2, k_p decreases quite steeply to negative values as f_c increases, and crosses zero for $f_c \approx 1.5$ Hz. The predicted force reflex gain is very small, which is also consistent with the experimental results.

There are, however, also particular differences. For NB noise type 1, k_p reaches zero around $f_h = 5$ Hz for the model prediction, and around $f_h = 3$ Hz for the experiments. Figure 7 shows that the resonant peak is already suppressed at $f_h = 2.3$ Hz in contrast to the model prediction where this peak is not suppressed before 5 Hz. For NB noise type 2 (Fig. 8) the resonant peak vanishes almost beyond 1.3 Hz. Furthermore, for all conditions the variation of the estimated k_v appears to be less pronounced than the predicted k_v, although there is a weak transition between positive and negative values for NB noise type 2. These differences suggest that the subjects prefer submaximal performance by smaller reflex gains, compared with the predicted reflex gains, which may be attributed to several factors:

1. The position signal of the manipulator may contain quite some power for $f > f_h$, due to the non-linear behaviour of the subject. However, this explanation is not likely since the experiments show highly linear behaviour which can be expected for small displacements.
2. The choice of the model constants is not likely to cause the differences between predicted and estimated behaviour, since they match the corresponding experimental values quite well.
3. The estimated behaviour is a reflection at endpoint level of the effects of underlying control processes at joint and muscle levels of shoulder and elbow, which are not described by the simplified model in the present paper. The model represents a set of muscle reflex gains by a single lumped reflex gain at the endpoint level. This simplification may result in differences between predicted and estimated reflex gains.
4. During the experiments, subjects may have weighted metabolic energy consumption, due to co-activation, to some extent. This results in a decrease in co-activation and, consequently, a decrease in the gain margin of the open-loop transfer function. This results in smaller reflex gains.
5. During the experiments, subjects may have weighted control effort, due to muscle activation by reflexive feedback, to some extent. This results in smaller reflex gains.

Consequently, it would be appropriate to perform a model analysis, similar to the present study but with the use of a more detailed arm model (Schouten et al. 2000). In this way, the effects of certain non-linearities (i.e. muscle dynamics, muscle activation dynamics, arm geometry, transducer dynamics), higher-order dynamics and the effects of control effort and energy considerations could be studied.

Furthermore, subjects will likely use their visual feedback for frequencies up to 1 Hz. The inclusion of visual feedback will be expected to improve the estimates into rather more realistic values for these lowest frequencies.

5.4 Implications

The basic agreement between the experimental and the theoretical results strongly suggests that during maximal performance posture tasks, the reflex gains are adapted by the CNS, in response to variations in the input frequency spectrum, in an optimal way. This conclusion is strictly valid for the 'minimize displacements' task instruction, in combination with small-amplitude stationary stochastic force inputs with rectangular power spectra. Nevertheless, the consistent adaptability of reflex gains by the CNS in response to different external stimuli is evident from this study.

The term 'impedance control', which is frequently used in postural control studies, is confusing. It suggests that the goal of the CNS is to attain a prespecified reference impedance, i.e. reference dynamics (e.g. Rozendaal 1997). However, the present study demonstrates that the goal of the CNS is rather to minimize a performance measure, such as the variance of the displacement, eventually weighted by measures of energy and control effort.

The response to wide-bandwidth inputs, or the step response, is not always useful as a criterion to adjust the controller parameters. A strongly undamped system is shown to be effective for narrow-bandwidth inputs which do not include the system's eigenfrequency (Figs. 5 and 6). Such a system reduces the relevant disturbance frequencies effectively, whereas the resonant frequencies do not occur, simply because they are not excited by the input signal.

6 Conclusions

The model predictions provide a clear explanation for the relation between the model parameters which affect the performance measure, the system stability, and the spectral bandwidth of the disturbance signal. The goal of the system is to maximize the performance, which corresponds to a minimization of the system response.

Due to time delays and activation dynamics in the reflexive feedback loops, substantial reflex gains decrease the stability margin amplifying the system's response at particular resonant frequencies, whereas they reduce the response at other frequencies. This property can be used to effectively suppress narrow-bandwidth disturbances which do not excite the resonant frequencies, especially when the system is close to boundary stability.

The predicted co-activation gain is maximal and independent of the input spectrum. This is consistent with the assumption in the separation method to estimate intrinsic and reflexive behaviour, yielding that the intrinsic dynamics are constant and independent of the input spectrum. Intrinsic feedback increases the system's stability margin and reduces the system response for all frequencies.

The predicted reflexive behaviour shows remarkable similarities with the estimated behaviour: (1) the predicted position reflex gain decreases gradually to zero with increasing bandwidth of the input; (2) for near-sinusoidal inputs with increasing center frequency, the predicted position reflex gain decreases steeply to negative values and crosses zero at about 1.5 Hz; and (3) the predicted force reflex gain is very small, which implies that force feedback does not contribute to increase the performance.

There are particular differences between estimated and predicted behaviour, likely suggesting that subjects prefer submaximal performance by smaller reflex gains, compared with the predicted reflex gains. This may be explained by several factors: (1) the estimated behaviour is a reflection at the endpoint level of the effects of underlying control processes at joint and muscle levels of shoulder and elbow; and (2) the subjects may have weighted metabolic energy consumption or control effort to some extent. Consequently, it would be appropriate to perform a model analysis, similar to the present study but with the use of a more detailed arm model. In this way, the effects of certain non-linearities, higher order dynamics and the effects of control effort and energy considerations could be studied.

The model simplifications in this study enable a very basic analysis of the different contributions of intrinsic and reflexive feedback to stability and performance in postural control. The basic principles appear to be consistent with reality, since the modelling and the experimental approach show essentially the same intrinsic and reflexive behaviour. The agreement between the experimental and the theoretical results strongly suggests that during maximal performance posture tasks, the reflex gains are adapted by the CNS, in response to variations in the input frequency spectrum, in an optimal way. Hereby, the CNS minimizes the variance of the displacements, rather than specifying the desired dynamical behaviour explicitly.

References

Agarwal GC, Gottlieb GL (1977a) Oscillation of the human ankle joint in response to applied sinusoidal torque on the foot. J Physiol (Lond) 268: 151–176

Agarwal GC, Gottlieb GL (1977b) Compliance of the human ankle joint. J Biomech Eng 99: 166–170

Agarwal GC, Gottlieb GL (1985) Mathematical modeling and simulation of the postural control loop: Part III. Crit Rev Biomed Eng 12: 49–93

Fitzpatrick RC, Gorman RB, Burke D, Gandevia SC (1992) Postural proprioceptive reflexes in standing human subjects: bandwidth of response and transmission characteristics. J Physiol (Lond) 458: 69–83

Hogan N (1984) Adaptive control of mechanical impedance by coactivation of antagonist muscles. IEEE Trans Autom Control 29: 681–690

Kearney RE, Hunter IW (1990) System identification of human joint dynamics. Crit Rev Biomed Eng 18: 55–87

Kirsch RF, Boskov D, Rymer WZ (1994) Muscle stiffness during transient and continuous movement of cat muscle: perturbation characteristics and physiological relevance. IEEE Trans Biomed Eng 41: 758–770

Marshall JE (1979) Control of time-delay systems. The Institution of Electrical Engineers, London, New York

McRuer DT, Jex HR (1967) A review of quasi-linear pilot models. IEEE Trans Hum Factors Electron 8: 231–249

Rozendaal LA (1997) Stability of the shoulder: intrinsic muscle properties and reflexive control. PhD thesis, Delft University of Technology, The Netherlands

Schouten AC, De Vlugt E, Van der Helm FCT, Brouwn GG (2000) Optimal posture control of a musculo-skeletal arm model. Biol Cybern (in press)

Stein RB, Oğuztöreli MN (1984) Modification of muscle responses by spinal circuitry. Neurosci 11: 231–240

Wieneke GH (1972) Variations in the output impedance of the human motor system. PhD thesis, University of Utrecht, The Netherlands

Winters JM, Stark L (1985) Analysis of fundamental human movement patterns through the use of in-depth antagonistic muscle models. IEEE Trans Biomed Eng 32: 826–839

Winters J, Stark L, Seif-Naraghi A (1988) An analysis of musculoskeletal system impedance. J Biomech 21: 1011–1025

Yurkovich S, Hoffmann K, Hemami H (1987) Stability and parameter studies of a stretch reflex loop model. IEEE Trans Biomed Eng 34: 547–553